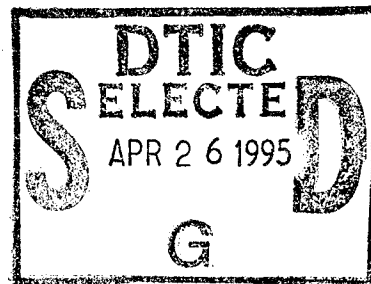


Iron Boltzmann Factor LIDAR: Proposed New Remote-Sensing Technique for Mesospheric Temperature

15 January 1995

Prepared by

J. A. GELBWACHS
Electronics Technology Center
Technology Operations



Prepared for

SPACE AND MISSILE SYSTEMS CENTER
AIR FORCE MATERIEL COMMAND
2430 E. El Segundo Boulevard
Los Angeles Air Force Base, CA 90245

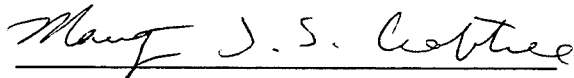
19950425 127

Engineering and Technology Group

This report was submitted by The Aerospace Corporation, El Segundo, CA 90245-4691, under Contract No. F04701-93-C-0094 with the Space and Missile Systems Center, 2430 E. El Segundo Blvd., Los Angeles Air Force Base, CA 90245. It was reviewed and approved for The Aerospace Corporation by T. Galantowicz, Principal Director, Electronics Technology Center.

This report has been reviewed by the Public Affairs Office (PAS) and is releasable to the National Technical Information Service (NTIS). At NTIS, it will be available to the general public, including foreign nationals.

This technical report has been reviewed and is approved for publication. Publication of this report does not constitute Air Force approval of the report's findings or conclusions. It is published only for the exchange and stimulation of ideas.

A handwritten signature in cursive script, reading "Maritza J. S. Crabtree".

Maritza Crabtree, Major USAF
SMC/CIE

REPORT DOCUMENTATION PAGE			Form Approved OMB No. 0704-0188	
Public reporting burden for this collection of information is estimated to average 1 hour per response, including the time for reviewing instructions, searching existing data sources, gathering and maintaining the data needed, and completing and reviewing the collection of information. Send comments regarding this burden estimate or any other aspect of this collection of information, including suggestions for reducing this burden to Washington Headquarters Services, Directorate for Information Operations and Reports, 1215 Jefferson Davis Highway, Suite 1204, Arlington, VA 22202-4302, and to the Office of Management and Budget, Paperwork Reduction Project (0704-0188), Washington, DC 20503.				
1. AGENCY USE ONLY (Leave blank)		2. REPORT DATE 15 January 1995		3. REPORT TYPE AND DATES COVERED
4. TITLE AND SUBTITLE Iron Boltzmann Factor LIDAR: Proposed New Remote-Sensing Technique for Mesospheric Temperature			5. FUNDING NUMBERS F04701-93-C-0094	
6. AUTHOR(S) Gelbwachs, Jerry A.				
7. PERFORMING ORGANIZATION NAME(S) AND ADDRESS(ES) The Aerospace Corporation El Segundo, California			8. PERFORMING ORGANIZATION REPORT NUMBER TR-94(4925)-1	
9. SPONSORING/MONITORING AGENCY NAME(S) AND ADDRESS(ES) Space and Missile Systems Center Air Force Materiel Command Los Angeles Air Force Base, CA 90245			10. SPONSORING/MONITORING AGENCY REPORT NUMBER SMC-TR-95-12	
11. SUPPLEMENTARY NOTES				
12a. DISTRIBUTION/AVAILABILITY STATEMENT Approved for public release; distribution unlimited.			12b. DISTRIBUTION CODE	
13. ABSTRACT (Maximum 200 words) We describe a new LIDAR technique for middle atmospheric temperature measurement. The proposed LIDAR exploits the Fe layer in the 80 - 100-km altitude region. Absolute temperatures are inferred by the use of the Maxwell-Boltzmann relationship from the ratio of LIDAR returns from mesospheric Fe atoms excited at 372 and 374 nm, corresponding to the ground-state resonance line and a thermally populated resonance line, respectively. The wavelengths of the new LIDAR are favorable for capturing Rayleigh signals from the middle atmosphere. A simulation indicates that a complete temperature profile from 30 to 100 km can be acquired with the proposed LIDAR by monitoring simultaneously the Rayleigh signals and the Fe fluorescence returns excited by the same transmitter pulse.				
14. SUBJECT TERMS LIDAR, mesospheric-temperature monitoring, remote sensing			15. NUMBER OF PAGES 10	
			16. PRICE CODE	
17. SECURITY CLASSIFICATION OF REPORT UNCLASSIFIED	18. SECURITY CLASSIFICATION OF THIS PAGE UNCLASSIFIED	19. SECURITY CLASSIFICATION OF ABSTRACT UNCLASSIFIED	20. LIMITATION OF ABSTRACT	

Contents

1.	Introduction	1
2.	Description of the Method	2
3.	Sensitivity to Temperature Change	3
4.	Anticipated Mesospheric Fe Signals	3
5.	Sensing Temperature at Lower Altitudes by the Use of Rayleigh LIDAR	4
6.	Comparison with Na Doppler Temperature LIDAR	5
7.	Summary	6
	References	6

Figures

1.	Partial energy-level diagram for atomic Fe	2
2.	Theoretical temperature sensitivity of the Fe Boltzmann factor LIDAR, the Na Doppler temperature LIDAR, and the Rayleigh LIDAR	3
3.	LIDAR simulation of the middle atmospheric signals expected at the primary Fe resonance line, the temperature-sensitive Fe resonance line, and the Rayleigh LIDAR	5

Tables

1.	Comparison of Upper Mesospheric Temperature LIDARs	5
----	--	---

Accession For	
NTIS CRA&I	<input checked="" type="checkbox"/>
DTIC TAB	<input type="checkbox"/>
Unannounced	<input type="checkbox"/>
Justification	
By	
Distribution /	
Availability Codes	
Dist	Avail and / or Special
A-1	

Iron Boltzmann factor LIDAR: proposed new remote-sensing technique for mesospheric temperature

Jerry A. Gelbwachs

We describe a new LIDAR technique for middle atmospheric temperature measurement. The proposed LIDAR exploits the Fe layer in the 80–100-km altitude region. Absolute temperatures are inferred by the use of the Maxwell-Boltzmann relationship from the ratio of LIDAR returns from mesospheric Fe atoms excited at 372 and 374 nm, corresponding to the ground-state resonance line and a thermally populated resonance line, respectively. The wavelengths of the new LIDAR are favorable for capturing Rayleigh signals from the middle atmosphere. A simulation indicates that a complete temperature profile from 30 to 100 km can be acquired with the proposed LIDAR by monitoring simultaneously the Rayleigh signals and the Fe fluorescence returns excited by the same transmitter pulse.

Key words: LIDAR, mesospheric-temperature monitoring, remote sensing.

1. Introduction

Knowledge of the temperature and density in the upper atmosphere is important for the understanding of a wide range of geophysical phenomena such as airglow, mesospheric temperature inversions, gravity wave breaking, and reentry effects and for discerning trends in global climate changes.¹ The standard meteorological techniques currently used in the United States for mesospheric-temperature measurements include datasonde rockets for measurements between 20 and 65 km and the falling passive sphere method for altitudes between 30 and 90 km. Recently, nadir-viewing satellites with onboard radiometric sensors have contributed to the acquisition of temperature profiles. However, these methods currently lack the accuracy and spatial resolution required for many of the above applications.

In recent years much progress has been made toward remote sensing of the upper atmosphere with LIDAR. The excellent accuracy and spatial resolution of LIDAR make it an ideal ground-based instrument for upper atmospheric monitoring and for calibration of sensors onboard satellites. Temperature measurements in the 30–90-km altitude region

have been recorded with Rayleigh LIDARs,² and LIDARs tuned to the sodium *D* line have provided useful temperature data in the 85–110-km range.³

Recently, groups in Europe and the United States reported observations of atomic Fe in the mesospheric metallic layer with LIDARs tuned to the 372-nm Fe resonance line.^{4–6} It has been determined that the Fe layer extends from 80 to 100 km. Yearly LIDAR measurements have recorded seasonal variations of the Fe densities and instances of sporadic enhancements. The permanent Fe layer appears to be centered near 88 km and has densities in excess of Na values in the metallic layer. Just as the existence of atomic Na in the mesosphere provided the impetus for the development of LIDAR methods that were used to infer atmospheric properties from the spectroscopy of Na, we began to search for ways that the presence of Fe in the metallic layer might be exploited for middle atmospheric temperature monitoring.

In this paper we describe a new LIDAR technique for temperature sensing based on optical interactions with free Fe atoms in the atmosphere. It is called the Fe Boltzmann factor LIDAR. We begin in Section 2 with a description of the proposed method, and we discuss its temperature sensitivity in Section 3. The anticipated mesospheric Fe signals excited by a moderate power solid-state LIDAR transmitter are calculated in Section 4. An intriguing feature of the new LIDAR method, namely, the capability of simultaneous acquisition of temperatures in the 30–80-km altitude region by the use of the Rayleigh method in

conjunction with the new technique, is then discussed in Section 5. In Section 6 we compare the Fe Boltzmann factor LIDAR with the Na Doppler temperature LIDAR.

2. Description of the Method

The technique for remotely sensing mesospheric temperatures is based on the spectroscopy of Fe. It can be best understood with the aid of Fig. 1, which displays a partial energy-level diagram of atomic Fe. The a^5D ground level is split into five components. The separation between the lowest-energy members of the ground-level quintet is 416 cm^{-1} . Both levels are optically coupled to the z^5F° level centered at 3.375 eV . The $z^5F^\circ - a^5D_4$ transition corresponds to 372 nm and is considered the primary resonance line. The $z^5F^\circ - a^5D_3$ transition occurs at 374 nm and is another resonance line. Both transitions possess moderate oscillator strengths, namely, 0.04 . When it is excited, the $J' = 5$ level decays by emission of resonance radiation. The $J' = 4$ level relaxes to the $J'' = 3$ and $J'' = 4$ levels by emission of radiation at 374 and 368 nm , respectively. The branching ratio of the 368-nm emission is 9% .⁷

Iron atoms in the mesosphere can be considered to be in thermal equilibrium with their surroundings. Hence the steady-state population in the ground-level $J'' = 3$ component is related to the population in the $J'' = 4$ level in accordance with the Maxwell-Boltzmann relationship,

$$n(J'' = 3)/n(J'' = 4) = (g_2/g_1)\exp(-\Delta E/kT), \quad (1)$$

where n is the level population, $g_{2,1}$ are the degeneracy factors of the $J'' = 3$ and $J'' = 4$ levels, respectively, ΔE is the energy separation of the two levels, k is Boltzmann's constant, and T is temperature.

The right-hand side of Eq. (1) is the well-known Boltzmann factor. From Eq. (1) we note that the

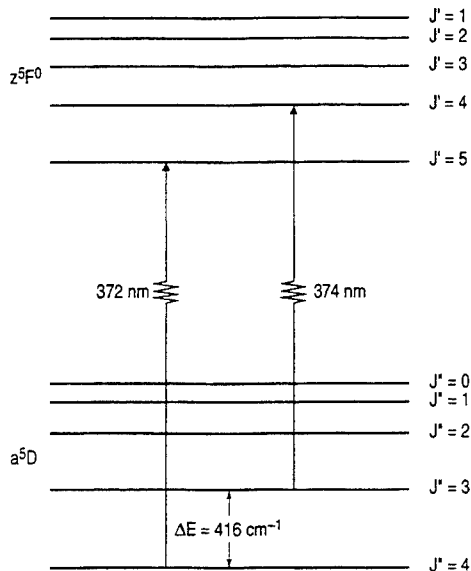


Fig. 1. Partial energy-level diagram for atomic Fe.

population ratio is a function of temperature alone. Thus the proposed new method for monitoring upper atmospheric temperature involves the transmission of laser pulses at 372 and 374 nm and the monitoring of the corresponding fluorescence returns. Absolute temperature is inferred from the ratio of the return signals with the Boltzmann factor. Hence we call the new remote-sensing technique the Fe Boltzmann factor LIDAR, or the Fe temperature LIDAR.

It is noted that at 200 K , a representative 88-km -altitude temperature, the Boltzmann factor corresponding to the 416-cm^{-1} energy separation between $J'' = 3$ and $J'' = 4$ is 0.039 . Thus 3.9% of the atomic Fe population resides in the $J'' = 3$ level. The energy separation in the ground level between the $J'' = 3$ and the $J'' = 2$ components is 288 cm^{-1} . From Eq. (1) we calculate that 0.3% of the atomic population is in the $J'' = 2$ level. We consider this population fraction to be negligible, and for the purpose of our subsequent analysis we ignore all a^5D level populations other than those residing in the lowest two levels.

Let us now derive the relationship between LIDAR signals and temperature. The LIDAR equation for zenith-viewing fluorescence LIDAR can be written as

$$S = (E/h\nu)n\sigma L(A_r/4\pi z^2)T_a^2 T_o \eta, \quad (2)$$

where S is the photoelectronic counts, E is the transmitter pulse energy, $h\nu$ is the photon energy at the transmitter wavelength, n is the density of the fluorescence species, σ is the absorption cross section, L is sample cell length or spatial resolution, A_r is the receiver area, z is the altitude, T_a is the one-way atmospheric transmission, T_o is the transmission through the receiver optics, and η is the photomultiplier (PMT) quantum efficiency.

Because of the reduced molecular density in the metallic layer, contributions to atomic-line broadening from collisions are much less than the spectral spread that is due to the thermal motion of the radiating atoms. Hence we assume for computational purposes that there are purely Doppler-broadened line shapes in the metallic layer. At 200 K the calculated Doppler linewidths (FWHM) for the Fe resonance lines of interest are 1.1 GHz . The Doppler-broadened absorption cross section is related to the Einstein transition probability A by

$$\sigma = (2/\Delta\nu_D)\sqrt{\ln 2}/\pi(\lambda^2/8\pi)(g_u/g_l)A, \quad (3)$$

where $\Delta\nu_D$ is the Doppler linewidth, λ is the wavelength, and $g_{u,l}$ are the degeneracy factors of the upper and lower levels, respectively. Substitution of Eqs. (1) and (3) into Eq. (2) yields

$$\begin{aligned} [S(\lambda_{\text{ex}} = 374 \text{ nm})/S(\lambda_{\text{ex}} = 372 \text{ nm})] \\ = (\lambda_2\sigma_2g_2/\lambda_1\sigma_1g_1)\exp(-\Delta E/kT). \end{aligned} \quad (4)$$

The spectroscopic parameters for the Fe transitions of interest are as follows⁷: $g_2 = 7$, $g_1 = 9$, $A(J' = 4) = 0.142 \times 10^8/\text{s}$, $A(J' = 5) = 0.163 \times 10^8/\text{s}$, $\sigma(374 \text{ nm}) = 8.78 \times 10^{-13} \text{ cm}^2$, and $\sigma(372 \text{ nm}) =$

$9.45 \times 10^{-13} \text{ cm}^2$. We calculated the cross sections of the Fe transitions by assuming that the linewidths were Doppler-broadened at 200 K. Substitution of the above values into Eq. (4) yields

$$\begin{aligned} [S(\lambda_{\text{ex}} = 374 \text{ nm})/S(\lambda_{\text{ex}} = 372 \text{ nm})] \\ = 0.73 \exp(-\Delta E/kT). \end{aligned} \quad (5)$$

When we substitute Eq. (3) into Eq. (4), it can be readily seen that the ratio of signals depends on ΔE , k , and the ratio of wavelengths, degeneracies, and transition probabilities. Hence the absolute accuracy of temperature measurement with the new LIDAR technique depends on the known accuracies of the above factors. With the exception of the transition probabilities, all the parameters are known to within 0.1%. The uncertainties associated with the transition probabilities of the $J' = 5$ and $J' = 4$ levels are approximately 10%; however, the relative accuracy of the two transition probabilities is less than 0.5%.⁸ Therefore the accuracy of the Fe Boltzmann factor LIDAR method is better than 1%.

3. Sensitivity to Temperature Change

An important consideration for a remote-sensing technique is its sensitivity to temperature change. We define temperature sensitivity S_T as the absolute value of the ratio of fractional change in the LIDAR signal to the fractional temperature change,

$$S_T \equiv |(\Delta S/S)|/|(\Delta T/T)|. \quad (6)$$

Let us now calculate this parameter for the Fe Boltzmann factor LIDAR. The calculation is greatly simplified by noting that the population in the lowest sublevel remains effectively constant over the temperature range of interest. Taking the derivative of Eq. (1) with respect to temperature under the approximation of fixed population in the $J'' = 4$ level, we can readily show that

$$dn(J'' = 3)/n(J'' = 3) = (\Delta E/kT)dT/T. \quad (7)$$

From Eq. (2) we note that the LIDAR signal is directly proportional to population. Thus the temperature sensitivity is simply the factor inside the parentheses on the right-hand side of Eq. (7). If we assume a mesospheric Fe temperature of 200 K, the temperature sensitivity equals 3.0. Hence a 1% temperature variation at 200 K will change the upper sublevel population, and hence the signal ratio, by 3%. In Fig. 2 we plot the theoretical temperature sensitivity as a function of the range of expected temperatures in the 80–100-km altitude region. It can be seen from Fig. 2 that S_T of the Fe Boltzmann factor LIDAR decreases monotonically from a maximum of 4.1 at 150 K to 2.2 at 250 K. Also plotted in Fig. 2 is the temperature sensitivity for existing middle atmospheric temperature LIDARs, namely, dual-wavelength Na Doppler temperature LIDAR and Rayleigh LIDAR. These LIDAR techniques are discussed below.

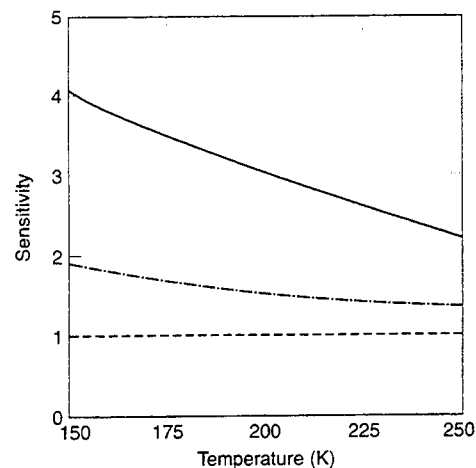


Fig. 2. Theoretical temperature sensitivity of the Fe Boltzmann factor LIDAR (solid curve), the Na Doppler temperature LIDAR (dotted-dashed curve), and the Rayleigh LIDAR (dashed line).

Temperature sensitivity plays an important role in the determination of the signal counts $S(\delta)$ that are required for the technique to achieve a prescribed temperature precision δ . If we assume that ideal Poissonian statistics are associated with the conversion of received photons into electronic pulses by the PMT, it is readily shown that

$$S(\delta) = (\delta S_T)^{-2}. \quad (8)$$

Implicit in Eq. (8) is the absence of background noise and PMT dark-current noise. Hence LIDAR techniques with high S_T require less integration time to achieve a specified temperature uncertainty.

4. Anticipated Mesospheric Fe Signals

In Section 4 we calculate returns from a moderate-power dual-wavelength LIDAR system operating at the Fe resonance wavelengths. The LIDAR equation for a zenith-viewing LIDAR that monitors Fe fluorescence signals originating in the mesosphere is given by Eq. (2). To calculate the return signals, a representative Fe density profile is needed. To my knowledge, the most extensive LIDAR observations of the Fe layer to date have been performed by a group at the University of Illinois at Urbana-Champaign (UIUC) in the fall of 1989 and the spring through fall of 1991.⁶ Therefore we use the UIUC-reported measurements for the representative atmospheric Fe parameters. During the observation period the Fe layer was centered at an altitude of 88.5 km and had a mean rms layer width of 3.0 km. The peak Fe densities varied from 1×10^4 atoms/cm³ in the summer to 3×10^4 atoms/cm³ in the spring and fall. Hence we assume an average value of 2×10^4 atoms/cm³ for our calculations. Let us posit the following system parameters for the 0.37- μm LIDAR: $E = 0.25 \text{ J/pulse}$, $A_r = 1 \text{ m}^2$, $L = 3 \text{ km}$, $T_a^2 = 0.2$, $T_o = 0.4$, and $\eta = 0.3$. Furthermore, we assume that the transmitter pulses are of a single frequency, with linewidths much less than the 1.1-GHz Doppler widths

of the Fe transitions. Substitution of the above values into Eq. (2) yields

$$S(\lambda_{\text{ex}} = 374 \text{ nm}) = 24 \text{ counts,}$$

$$S(\lambda_{\text{ex}} = 372 \text{ nm}) = 670 \text{ counts.}$$

Let us now calculate the integration time required for the system to achieve temperature measurements with 1% precision. When we substitute the appropriate values for the Fe Boltzmann factor LIDAR into Eq. (8), we find that 1.1×10^3 counts at $\lambda_{\text{ex}} = 374 \text{ nm}$ are necessary, which corresponds to 46 pulse pairs. If we assume that the system operates at a 10-Hz rate, the requisite counts will be accumulated in 9 s. Because the signal at $\lambda_{\text{ex}} = 372 \text{ nm}$ is much larger than the $\lambda_{\text{ex}} = 374 \text{ nm}$ return, its uncertainty will be much smaller and, hence, has been ignored in the error analysis.

The LIDAR performance described above predicates a 250-mJ laser system tunable between 372 and 374 nm. Additionally, the system must be capable of producing single-frequency pulses with excellent pulse-to-pulse frequency stability to overlap the 1.1-GHz-wide Doppler-broadened Fe resonance lines. Previous measurements of the Fe layer used single-frequency dye lasers that generated 10–25 mJ per pulse, with linewidths greater than the Fe Doppler widths.^{4–6} This amount of energy, although suitable for mapping the Fe layer density profiles by excitation of the strong 372-nm resonance line, needs to be scaled by at least an order of magnitude to monitor the smaller signals emanating from the temperature-sensitive resonance line. It may be difficult to scale dye laser output energies to higher values while preserving good frequency stability because of thermal and photochemical problems associated with the operation of dye lasers. Fortunately, tunable solid-state laser systems that can achieve the requisite performance are being developed. Appropriate candidate laser systems include frequency-doubled alexandrite and titanium-sapphire lasers. Injection locking the oscillators with the output of highly stable diode lasers has been demonstrated, and this technique can provide stable single-frequency operation. Recent developments in optical parametric oscillators suggest that they, too, may be suitable candidates.

The new temperature-measurement technique can be implemented in a variety of ways. In one method a 368–374-nm passband optical filter is placed in front of the photodetector. This filter blocks out skylight and eliminates the need to change filters when the transmitter wavelength is switched between resonance lines. Accurate temperature measurements require the accumulation of signal counts at each wavelength for a time period over which the Fe density is stationary. This time interval has not been directly determined. Because the dynamics of the Na layer is similar to that of the Fe layer, a good estimate of this duration is the corresponding period for the Na layer, namely, several minutes. Hence transmitter wavelengths can be switched between

shots or up to once every few minutes. Alternatively, an asymmetric transmission sequence can improve precision by preferential collection of the weaker signal. In this scheme, transmission of 374-nm pulses consumes greater than 50% of the transmission duty cycle. Because the return from the thermally populated resonance line is anticipated to be less than 10% of the signal excited at 372 nm, one may elect to project 374-nm pulses during ~90% of the duty cycle.

5. Sensing Temperature at Lower Altitudes by the Use of Rayleigh LIDAR

To date, the most successful LIDAR technique for monitoring temperature in the 30–90-km range is Rayleigh LIDAR.⁹ With this method the elastic-scattered return from atmospheric nitrogen and oxygen is converted into temperature data based on the assumption of hydrostatic equilibrium and the ideal gas law. Excellent Rayleigh data have been obtained with frequency-doubled Nd:YAG transmitters at 532 nm and with XeF excimer lasers operating at 351 nm.³ Because of the rapid decline of atmospheric density with altitude, it is very difficult to obtain high-precision temperature measurements with Rayleigh LIDAR beyond 80 km. Scattering from stratospheric aerosols provides background interference for Rayleigh LIDAR, thereby impeding its usage at lower altitudes. It is readily shown from the ideal gas law that the temperature sensitivity of the Rayleigh technique is equal to 1.

Because the proposed Fe Boltzmann factor LIDAR monitors signals with high precision from 80 to 100 km, it is natural to contemplate its simultaneous usage as a Rayleigh LIDAR at lower altitudes. In this manner a complete temperature profile could be acquired throughout the 30–100-km altitude range. The encouragement to pursue this line of investigation was derived from Rayleigh LIDAR wavelength-optimization studies. When the wavelength dependence of the Rayleigh backscattering cross section, atmospheric transmission, and PMT quantum efficiency have been considered, it has been determined that the optimum spectral region for middle atmospheric Rayleigh LIDAR is 0.36–0.41 μm .¹⁰ The wavelengths of the Fe temperature LIDAR fall within this spectral range.

The simulated performance of the proposed dual-wavelength Fe LIDAR is shown in Fig. 3, in which the single-shot Fe fluorescence returns excited at 372 nm (solid curve) and 374 nm (dashed-dotted curve) and the Rayleigh signals for the 30–100-km altitude region are plotted. The system parameters for the Fe Boltzmann factor LIDAR are those values described above. Model atmospheric densities and temperatures were used in the Rayleigh simulation and to compute the Fe signals at the thermally populated resonance line.¹¹ We calculated the Rayleigh backscattering cross section from measured values at 337.1 nm and scaled it to 372 nm with a λ^{-4} factor. A representative Fe density profile was taken from a

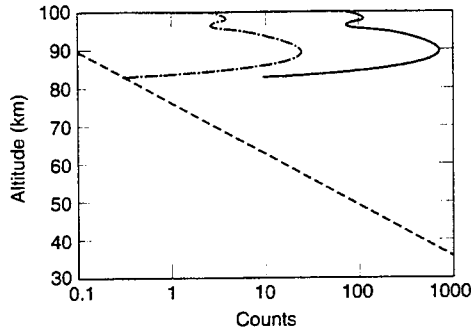


Fig. 3. LIDAR simulation of the middle atmospheric signals expected at the primary Fe resonance line (solid curve), the temperature-sensitive Fe resonance line (dashed-dotted curve), and the Rayleigh LIDAR (dashed curve).

recent study at UIUC (16 April data in figure 1 of Ref. 6). The maximum Fe density in this profile was $2.1 \times 10^4 \text{ cm}^{-3}$. We observe from Fig. 3 that the Rayleigh returns from the lower mesosphere are of comparable magnitude to the Fe signals at the higher altitudes, a result that is independent of system parameters. This important finding suggests that a complete temperature profile from 30 to 100 km can be obtained from the analysis of returns from a single LIDAR operating on the Fe resonance lines.

Another significant advantage of this technique is noted: because Rayleigh and Fe fluorescence signals can be obtained at the same altitude, temperature inferred from the Fe densities can serve as a high-end-point absolute calibration for the Rayleigh LIDAR measurements.

6. Comparison with NA Doppler Temperature LIDAR

The well-known Na layer in the upper mesosphere has been exploited by the use of LIDAR to monitor temperature. Two Doppler techniques have yielded measurements in the 80–100-km altitude range. Both methods involve excitation of the strong D_2 resonance line near 589 nm and monitoring of the subsequent fluorescence emission. Fricke and von Zahn scanned over the Doppler profile with an excimer-pumped dye laser and obtained Na temperature profiles with 1-km resolution and 10 K accuracy.¹² More recently, She *et al.* used a stabilized dye laser oscillator–amplifier system to measure temperatures between 82 and 102 km, with 1-km resolution and 3 K accuracy.¹³ In the latter method the hyperfine-split

Doppler line is probed with optical pulses at two precisely controlled wavelengths, the first pulse tuned near the peak of the line shape and the second pulse locked on to the crossover resonance located 0.85 GHz away. The ratio of returns is temperature sensitive. At 200 K the ratio is approximately 0.3 and the temperature sensitivity is 1.53. Over the 150–250 K range the temperature sensitivity varies from 1.90 to 1.36, as shown in Fig. 2. A comparison of mesospheric temperature LIDARs appears in Table 1.

We now compare the transmitter power P required for monitoring temperature with equal precision for the dual-wavelength Na LIDAR and the Fe LIDAR. Our analysis is simplified by noting that the uncertainties associated with the signals at the stronger wavelengths are much smaller than the uncertainties of the signals at the weaker lines, and hence the former can be ignored. The comparison is facilitated by Eq. (2). Keeping only the factors that are significantly different for the two LIDARs, we arrive at a simple expression for the power ratio,

$$\begin{aligned} P(374 \text{ nm})/P(589 \text{ nm}) \\ = [n_{\text{Fe}}(J'' = 3)\sigma(374 \text{ nm})\eta(374 \text{ nm})] \\ / [n_{\text{Na}}\sigma_c(589 \text{ nm})\eta(589 \text{ nm})]. \quad (9) \end{aligned}$$

The values of the parameters in Eq. (8) are as follows: $n_{\text{Fe}}(J'' = 3) = 7 \times 10^2 \text{ cm}^{-3}$, $\sigma(374 \text{ nm}) = 8.8 \times 10^{-13} \text{ cm}^2$, $\eta(374 \text{ nm}) = 0.3$, $n_{\text{Na}} = 5 \times 10^3 \text{ cm}^{-3}$, $\sigma_c = 3 \times 10^{-12} \text{ cm}^2$, and $\eta(589 \text{ nm}) = 0.12$. Substitution of the above values into Eq. (9) yields a power ratio of 10. Thus power an order of magnitude greater than that of the Na Doppler LIDAR is required for the Fe Boltzmann factor LIDAR to obtain similar signal levels at their respective weaker lines. To obtain identical measurement precision for the two methods, we need to modify the respective weak signal levels to account for differences in temperature sensitivity. When this adjustment is made, we find that the Fe LIDAR requires 2.6 times the power of the Na LIDAR.

We have considered the extension of the 589-nm LIDAR for remote temperature measurement at lower altitudes by the use of the Rayleigh technique, as was done in Section 5 for the Fe LIDAR. Compared with the Fe LIDAR, our calculations reveal stronger Na fluorescence signals in the 80–100-km region and

Table 1. Comparison of Upper Mesospheric Temperature LIDARs

Parameter	Fe		Na		Rayleigh
	Strong Line	Weak Line	Strong Line	Weak Line	
Wavelength (nm)	371.99	373.71	589.159	589.158	532
Typical density near 90 km (cm^{-3})	2×10^4	7.8×10^2	5×10^3		7×10^{13}
Cross section (cm^2) at 200 K	9.5×10^{-13}	8.8×10^{-13}	9.5×10^{-12}	2.8×10^{-12}	8.4×10^{-27}
Temperature sensitivity near 200 K		3.0		1.53	1.0
Counts at weaker line for 1% temperature precision	—	1.1×10^3	—	4.2×10^3	10^4
Rayleigh LIDAR efficiency		1.0		0.15	0.25

weaker Rayleigh returns at the lower altitudes for identical pulse energies and collection apertures. The large disparity between the Na signals and the Rayleigh signals indicates that coupling of the two LIDAR methods at 589 nm to acquire a complete mesospheric temperature profile is impractical. Limited field measurements support this conclusion.³

Two additional advantages of the Fe LIDAR compared with the Na LIDAR accrue from operation at near-UV wavelengths versus visible wavelengths. They are improved eye safety and reduced sky background.

7. Summary

We have developed a new LIDAR concept for absolute temperature measurement in the 80–100-km altitude region. The dual-wavelength Fe Boltzmann factor temperature-measurement method involves excitation of atomic Fe in the mesosphere at its 372- and 374-nm resonance lines. The proposed technique is highly sensitive to temperature and is compatible with tunable solid-state transmitters. Because the wavelengths of the Fe temperature LIDAR fall in the spectral region that is optimum for Rayleigh LIDAR, the new LIDAR offers the additional capability of sensing temperatures in the 30–80-km range by the use of the Rayleigh technique, thereby providing temperature profiles throughout the entire 30–100-km altitude region.

This work was performed under U.S. Air Force contract FO4701-93-C-0094.

References

1. J. T. Houghton, *The Physics of Atmospheres* (Cambridge U. Press, Cambridge, 1986).
2. A. Hauchercorne, M. L. Chanin, P. Keckhut, and P. Nedeljkovic, "LIDAR monitoring of the temperature in the middle and lower atmosphere," *Appl. Phys. B* **55**, 29–34 (1992).
3. C. S. Gardner, "Sodium resonance fluorescence LIDAR applications in atmospheric science and astronomy," *Proc. IEEE* **77**, 408–418 (1989).
4. C. Grainer, J. P. Jegou, and G. Megie, "Iron atoms and metallic species in the Earth's upper atmosphere," *Geophys. Res. Lett.* **16**, 243–246 (1989).
5. M. Alpers, J. Hoffner, and U. von Zahn, "Iron atom densities in the polar mesosphere from LIDAR observations," *Geophys. Res. Lett.* **17**, 2345–2348 (1990).
6. T. J. Kane, P. H. Mui, and C. S. Gardner, "Evidence for substantial seasonal variations in the structure of the mesospheric Fe layer," *Geophys. Res. Lett.* **19**, 405–408 (1992).
7. W. L. Wiese and G. A. Martin, "Wavelengths and transition probabilities for atoms and atomic ions," *Nat. Stand. Ref. Data Ser.* 68, (National Bureau of Standards, Washington, D.C., 1980).
8. J. R. Fuhr, National Institute of Standards and Technology, Gaithersburg, Md. 20899 (personal communication, October 1993).
9. M. L. Chanin and A. Hauchercorne, "LIDAR observation of gravity and tidal waves in the stratosphere and mesosphere," *J. Geophys. Res.* **86**, 9715–9721 (1981).
10. P. Keckhut, A. Hauchercorne, and M. L. Chanin, "A critical review of the data base acquired for long term surveillance of the middle atmosphere by the french rayleigh LIDARs," *J. Atmos. Oceanic Technol.* **10**, 850–867 (1993).
11. *U.S. Standard Atmosphere* (National Oceanic and Atmospheric Administration, Washington, D.C., 1976).
12. K. H. Fricke and U. von Zahn, "Mesopause temperature derived from probing the hyperfine structure of the D_2 resonance line of sodium by LIDAR," *J. Atmos. Terr. Phys.* **47**, 499–512 (1985).
13. C. Y. She, J. R. Yu, H. Latifi, and R. E. Bills, "High-spectral-resolution fluorescence light detection and ranging for mesospheric sodium temperature measurements," *Appl. Opt.* **31**, 2095–2106 (1992).

TECHNOLOGY OPERATIONS

The Aerospace Corporation functions as an "architect-engineer" for national security programs, specializing in advanced military space systems. The Corporation's Technology Operations supports the effective and timely development and operation of national security systems through scientific research and the application of advanced technology. Vital to the success of the Corporation is the technical staff's wide-ranging expertise and its ability to stay abreast of new technological developments and program support issues associated with rapidly evolving space systems. Contributing capabilities are provided by these individual Technology Centers:

Electronics Technology Center: Microelectronics, VLSI reliability, failure analysis, solid-state device physics, compound semiconductors, radiation effects, infrared and CCD detector devices, Micro-Electro-Mechanical Systems (MEMS), and data storage and display technologies; lasers and electro-optics, solid state laser design, micro-optics, optical communications, and fiber optic sensors; atomic frequency standards, applied laser spectroscopy, laser chemistry, atmospheric propagation and beam control, LIDAR/LADAR remote sensing; solar cell and array testing and evaluation, battery electrochemistry, battery testing and evaluation.

Mechanics and Materials Technology Center: Evaluation and characterization of new materials: metals, alloys, ceramics, polymers and their composites, and new forms of carbon; development and analysis of thin films and deposition techniques; nondestructive evaluation, component failure analysis and reliability; fracture mechanics and stress corrosion; development and evaluation of hardened components; analysis and evaluation of materials at cryogenic and elevated temperatures; launch vehicle and reentry fluid mechanics, heat transfer and flight dynamics; chemical and electric propulsion; spacecraft structural mechanics, spacecraft survivability and vulnerability assessment; contamination, thermal and structural control; high temperature thermomechanics, gas kinetics and radiation; lubrication and surface phenomena.

Space and Environment Technology Center: Magnetospheric, auroral and cosmic ray physics, wave-particle interactions, magnetospheric plasma waves; atmospheric and ionospheric physics, density and composition of the upper atmosphere, remote sensing using atmospheric radiation; solar physics, infrared astronomy, infrared signature analysis; effects of solar activity, magnetic storms and nuclear explosions on the earth's atmosphere, ionosphere and magnetosphere; effects of electromagnetic and particulate radiations on space systems; space instrumentation; propellant chemistry, chemical dynamics, environmental chemistry, trace detection; atmospheric chemical reactions, atmospheric optics, light scattering, state-specific chemical reactions and radiative signatures of missile plumes, and sensor out-of-field-of-view rejection.